An Investigation into the Effects of the Reynolds Number on High-Speed Trains Using a Low Temperature Wind Tunnel Test Facility

Yundong Han[1], Dawei Chen[1], Shaoqing Liu[1] and Gang Xu[2]

Abstract: A series of tests have been conducted using a Cryogenic Wind Tunnel to study the effect of Reynolds number (Re) on the aerodynamic force and surface pressure experienced by a high speed train. The test Reynolds number has been varied from 1 million to 10 million, which is the highest Reynolds number a wind tunnel has ever achieved for a train test. According to our results, the drag coefficient of the leading car decreases with higher Reynolds number for yaw angles up to 30º. The drag force coefficient drops about 0.06 when Re is raised from 1 million to 10 million. The side force is caused by the high pressure at the windward side and the low pressure generated by the vortex at the lee side. Both pressure distributions are not appreciably affected by Reynolds number changes at yaw angles up to 30º. The lift force coefficient increases with higher Re, though the change is small. At a yaw angle of zero the down force coefficient is reduced by a scale factor of about 0.03 when the Reynolds number is raised over the considered range. At higher yaw angles the lift force coefficient is reduced about 0.1. Similar to the side force coefficient, the rolling moment coefficient does not change much with Re. The magnitude of the pitching moment coefficient increases with higher Re. This indicates that the load on the front bogie is higher at higher Reynolds numbers. The yawing moment coefficient increases with Re. This effect is more evident at higher yaw angles. The yawing moment coefficient increases by about 6% when Re is raised from 1 million to 10 million. The influence of Re on the rolling moment coefficient around the leeward rail is relatively smaller. It increases by about 2% over the considered range of Re.

Keywords: High-speed train, wind tunnel test, reynolds number effect, aerodynamic performance, yaw angle.

1 Introduction

The high-speed railway in China accounts for 20,000 km in 2016. It will reach 38,000 km in 2025. Therefore, even a small improvement of the high speed train performance would have immense consequence. For high speed trains their aerodynamic characteristics have

a great influence on their performance. More than 70% of the traction effort is lost due to aerodynamic drag. By reducing the drag by 25%, it is possible to save up to 15% of traction energy. The cross-wind stability is influenced by aerodynamic forces and moments, especially the side force, lift and rolling moment. With increasing velocity the cross-wind stability decreases.

One of the most widely used methods for studying the characteristics of train aerodynamics is the model test. This has many advantages, such as mature test theory and experimental tools, and precise measurement technology. The flow parameters (such as speed and pressure) are easy to control and are not affected by weather changes. The problem is the Reynolds number effect. Due to the use of the scaled model, the Reynolds number for the test is much smaller than the corresponding full-scale value [Li, Hemida, Zhang et al. (2018)].

The Reynolds number is defined as the ratio of inertial forces and viscous forces, and consequently quantifies the relative importance of these two types of forces for a given set of flow conditions. All the flow phenomena related to viscosity, such as the boundary layer flow state, the transition and the separation point, the minimum drag coefficient and maximum lift coefficient are dependent on Reynolds number [Barre and Barnaud (1995)]; it is one of the important criteria of similarity, characterizing the impact of viscosity on the flow.

It is found that the influence of the Reynolds number on the aerodynamic forces, pressures and other parameters is relatively small if it is high enough. This range is called as self-simulation range. No accurate conclusions have been drawn regarding the scope and the impact of the self-simulation range, or the reliability of using the model test results for the full-scale. This issue has caused widespread concern among experts and scholars, although few research results have been published. The lift force has been found by Baker et al. [Baker and Humphreys (1996)] to be sensitive to the Reynolds number and in particular to the ground simulation in the wind tunnel. The sensitivity of the longitudinal slip stream profiles to Reynolds number is presented by Bell et al. [Bell, Burton and Thompson (2014)].

It has long been recognized that the Reynolds number has an influence on many of the aerodynamic characteristics of a train; however, in the actual design process, the Reynolds number is considered to have impact only within the boundary layer. Reynolds number has influence solely on the friction and maximum lift coefficient [Schewe (2001)]. In practice, the wind tunnel test data at low Reynolds numbers are used directly, and only the drag coefficient is corrected. When extrapolating the wind tunnel test results, only the effect on the maximum lift coefficient and friction coefficient are considered; past experience has proved that this treatment will not cause large errors.

Some scholars have carried out wind tunnel test on the influence of Reynolds number on the aerodynamic performance of high-speed trains [Niu, Liang and Zhou (2016)]. The results are based on the room temperature wind tunnel test. The Reynolds number obtained by the test is much lower than that of the real car. Because of the shrinkage wind tunnel test, the Reynolds number obtained by the test is quite different from the actual train Reynolds number. In this paper, using the low temperature wind tunnel test technology, the wind tunnel test results closer to the real vehicle Reynolds number can be obtained, and the test results are more realistic and accurate.

The European Standard EN14067-6 "Requirements and test procedures for cross wind assessment" [CEN (2010)] demands that the test Reynolds number shall be higher than 600,000 (DB RIL 80704) or 250,000 (RSSB standard GM/RC2542). The Reynolds number dependency shall be checked. According to RSSB standard if the lee rail rolling moment coefficient varies by less than ±5% over range [$0.9Re_{max}$; Re_{max}], the test data are considered to be Reynolds number independent.

However, with the continuous development of high-speed trains, it is required to predict their aerodynamic characteristic precisely. This means for the model test that the testing Reynolds number shall be as close to the running Reynolds number as possible. This could be obtained by testing train models at high Reynolds wind tunnels, such as a cryogenic wind tunnel. Due to the relatively high costs of performing test at cryogenic wind tunnels, it is desirable to find a way to correct the test data at low Reynolds numbers to full-scale.

The purposes of this paper was to investigate the influence of the Reynolds number on the wind tunnel train test and to determine a proper test Reynolds number for the wind tunnel train test so that the wind tunnel test data can be used for full-scale.

For this purpose a model of a high-speed train that is already in operation in China was tested in a cryogenic wind tunnel at various Reynolds numbers. The model is designated as Model A in this paper.

2 Methodology

2.1 Cryogenic wind tunnel test technique

The measurements have been carried out in the DNW Cryogenic wind tunnel (KKK) in Cologne Germany. A sketch of the wind tunnel is shown on Fig. 1. The Cryogenic Wind Tunnel Cologne (KKK) is a closed circuit low speed tunnel. To achieve high Reynolds numbers, the gas temperature in the tunnel circuit can be lowered down to 100 K by injecting liquid nitrogen. The Reynolds-number can thus be increased by a factor of 5.5 while the drive power remains constant as shown in Fig. 2. Due to the possibility of independent variation of the gas temperature and flow velocity, the influence of the Mach number and Reynolds number on the aerodynamic characteristics can be investigated separately. Tunnel operation, test parameters, and the measurement and data acquisition are automatically controlled by an integrated hard- and software system.

The test section area consists of the test section itself, the model access lock and the model conditioning room. Both sidewalls of the test section are equipped with two rows of windows each enables the application of flow visualization and optical measurement techniques. The access lock and the model conditioning room are located underneath the test section. They allow model changes at ambient temperature while the tunnel is maintained at cryogenic temperature. In this way high productivity can be achieved.

The model access lock and the model conditioning room both have individual temperature control systems provided by nitrogen and dry air injection and enforced heating. In this manner they can also be used as independent cryogenic (pre-) test facilities.
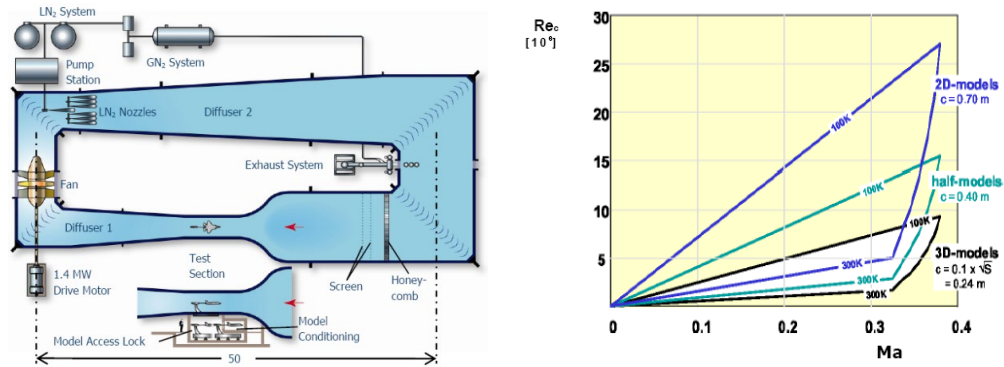
Figure 1: Sketch of the cryogenic wind tunnel **Figure 2:** Mach und Re capabilities of KKK

Due to its Re-Ma-capability the KKK is an outstanding wind tunnel for high-speed train testing. It was qualified for train testing according to EN14067-6. The performances and reliability of the DNW Cryogenic wind tunnel (KKK) in Cologne Germany can be confirmed by the published literature such as Becker et al. [Becker, Zhai, Rebstock et al. (2003); Becker, Rebstock, Loose et al. (2005)] and Ahlefeldt et al. [Ahlefeldt and Koop (2010)].

The measurements described in the following were performed using an internal 6-component balance. This is a cold balance. It can work from ambient to cryogenic conditions.

A temperature compensated electronic pressure scanning system (PSI) was used for pressure measurements.

The model was installed on a 3.1×1.3×0.03 m splitter plate located 185 mm above the wind tunnel floor in order to be outside of the wind tunnel boundary layer. This setup allows a fresh boundary layer on the splitter plate which is small enough compared to the model height. Some distances between plate border and the center of rotation are shown on Fig. 3.

The boundary layer thickness on the plate was determined using the turbulent boundary layer thickness equation of a flat plate. The value is somewhat higher than that in reality, because the boundary layer is laminar at the leading edge of the plate. The boundary layer thickness at three positions as shown in Fig. 4 was calculated at Reynolds number from 1 million to 10 million.
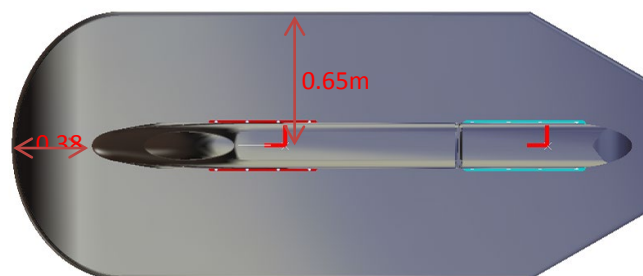

Figure 3: Distance between splitter plate border and center of rotation and train model
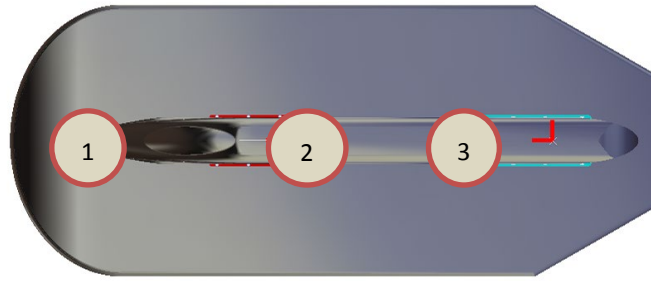
Figure 4: Locations to determine the BL thickness

The boundary layer thickness on the splitter plate grows with increasing distances from the leading edge and decreases with the Reynolds number. The values are shown in Fig. 5. The maximum boundary layer thickness at the axis of rotation (position 2) is around 22 mm which represents 8.1% of the model height. The value is below the maximum value of 30% as requested by the EN14067-6 [CEN (2010)].
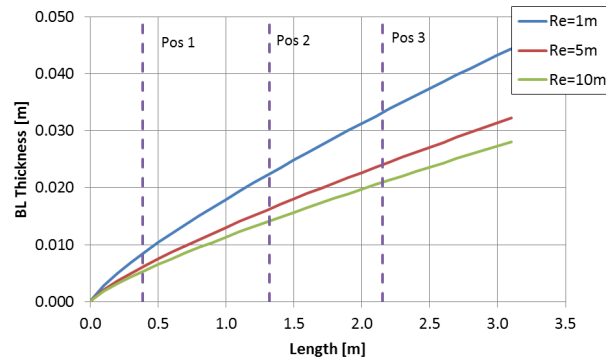

Figure 5: Theoretical flat plate boundary layer thickness (Re∞: 1×106, 5×106 and 10×106)

The measurements described in this report were performed at different Reynolds numbers in order to investigate the Reynolds number effect. The Reynolds number is defined by Li et al. [Li, Zhang, Mohammad et al. (2019)]:

$$R_e = \frac{U d_0}{v} \tag{1}$$

where U is the tunnel velocity in the test section, v the kinematic viscosity and d_0 the characteristic length. For the 1:15 scaled reference model ICE3 the reference length is 0.2 m (3 m for a full scale train).

For Model A the height is defined as characteristic length. The characteristic length is therefore 0.27 m for the 1:15 scaled model (4.05 m for a full scale train).

The measurements in the cryogenic wind tunnel (KKK) enable the independent investigation of the Reynolds number and Mach number influence on the aerodynamic force, moment and pressure coefficients. Besides, changing blockage ratios due to the

variation of the yaw angle and slight temperature variations were compensated by Mach number adjustments.

$$M_a = \frac{U}{c} \tag{2}$$

The Mach number is defined above with U the tunnel velocity and c the speed of sound.

The air density $\rho = p/(RT)$ is calculated from the average measured temperature T and the static pressure p for each test using the ideal gas law with an specific gas constant R of 297 J/(kg·K). The temperature T is measured using a temperature sensor Pt100 in the test section and the static pressure p is measured using a Prandtl probe in the test Section.

The blockage ratio is defined as the ratio of the projected area of the model, the splitter plate with its support and the test section. For a yaw angle of 30°, the blocking ratio corresponds to 8.3% for the test model.

The blockage in the KKK closed test section at yaw angle of 30° in flat ground configuration is below 15% which implies that no blockage correction has to be applied in agreement with EN14067-6 [CEN (2010)].

Nevertheless, to have a more realistic result, the corrected result is also presented. The blockage correction method in EN14067-6 [CEN (2010)] was applied. A Prandtl probe (Fig. 6) is mounted 360 mm away from the tunnel ceiling to measure the dynamic pressure at each yaw angle. The coefficients that are normalized using this dynamic pressure are then the blockage corrected values.

Figure 6: Prandtl pitot probe for the blockage correction

2.2 Experimental setup and model

The simulation of the flow between a stationary train model and ground in a wind tunnel is difficult, because in a wind tunnel the model and the ground undergo the same wind velocity, while in reality a train runs over a rail. To simplify the train test in a wind tunnel, EN14067-6 [CEN (2010)] has defined three ground configurations: flat ground, single track and ballast, and embankment of 6 m height.

For the flat ground configuration (Fig. 7), the simulation of the ballast and rails is omitted, thus the unrealistic effect of the rail is eliminated. This configuration is a better compromise. The flat ground configuration was chosen for this investigation.
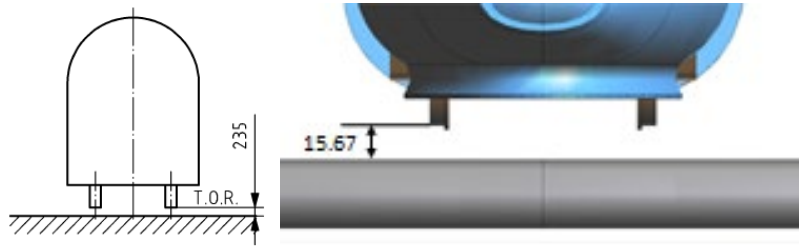
Figure 7: Sketch of the wind tunnel configuration flat ground with 235 mm gap

As mentioned before, wind tunnel measurements were performed with 1:15 scaled train models. The benchmark model ICE3, as shown in Fig. 8, consists of a leading car and a downstream body. The leading car is fixed to the splitter plate via an internal six-component balance, balance adapter and four struts. The downstream body is smaller than half the length of the leading car and is fixed to the splitter plate via four struts. There is a 4 mm gap between the leading car and the downstream body to prevent any contact between the measured car and downstream body during the measurements. The bogie is simplified, but preserves its aerodynamic characteristics.

This model was manufactured of synthetic materials with strengthening core of an aluminum profile. It has a high surface quality. The complete model geometry was manufactured in accordance with requirements specified in EN14067-6 [CEN (2010)].

Figure 8: Benchmark model ICE3   **Figure 9:** Wind tunnel model A

The Model A is shown in Fig. 9. It is composed of a leading car and a downstream body. The downstream body is one half of the middle car. Its end is smoothed with an elliptical surface. The model is equipped with three bogies (Fig. 10): two driving bogies and one towing bogie. The bogies were modelled as a symmetrical structure.

The model was manufactured of aluminum alloy. This material satisfies strength, toughness and form stability requirements at cryogenic conditions. The model was equipped with 59 pressure taps. Each pressure tap has a diameter of 0.3 mm.

The model geometry accuracy was examined. The maximal geometrical deviation of the leading car is 0.078 mm. The deviation of the downstream body is 0.096 mm. They are far better than the required 0.67 mm (10 mm/15). The maximal surface roughness Ra is 0.451 μm. The admissible roughness is given as:

$$k_s = \frac{100 d_0}{R_e} \tag{3}$$

The admissible roughness for Model A with a reference length of 0.27 m at Reynolds number of 10 million is 2.7 μm. Therefore, the surface quality requirement is satisfied.
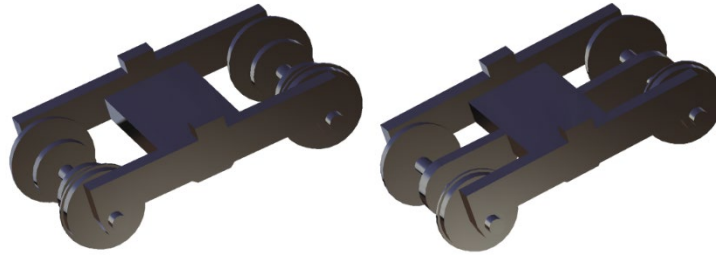
Figure 10: Detailed bogies of model A

2.3 Wind tunnel instrumentation

In order to measure the aerodynamic force and moment the model was equipped with an internal six-component balance. One side of the balance was fixed to the model whereas the other side was fixed to the splitter plate via a balance adaptor and four struts as shown in Fig. 11.

Figure 11: Location of internal balance in the model

The balance (Fig. 12) was manufactured of Maraging steel 250. This steel has a high strength and retains its toughness at cryogenic conditions. Its dimension is completely stable from ambient temperature to cryogenic conditions. From the view point of measurement, it has small hysteresis and creep. The balance structure was optimized, so that it has a high sensitivity and at the same time high stiffness, especially it is not sensitive to the temperature gradients in the balance. The strain gages in each bridge were matched, so that the electrical zero drift was small.

During the wind tunnel test the balance follows the tunnel temperature. Its working temperature ranges from ambient to cryogenic.

This balance is instrumented with 7 strain gauge bridges. Two of these are used for the axial force measurement. The rest 5 bridges are used for the measurement of the side force, the lift force, the rolling, pitching and yawing moment, respectively.
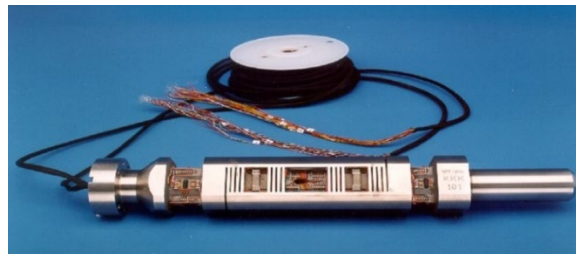

Figure 12: The KKK balance W614

The 95% confidential intervals of the balance at different temperatures are listed in Tab. 1. If the uncertainty of the dynamic pressure is taken into account, the maximal uncertainty of the axial force coefficient is estimated to be 0.001. The uncertainty of the side force and lift coefficient comes to 0.002. The uncertainty of the three moment coefficients is smaller than 0.0005.

Table 1: 95% confidence intervals of the balance [%FS]

Temperature [K]	Fx	Fy	Fz	Mx	My	Mz
295	0.03	0.03	0.02	0.04	0.02	0.02
240	0.04	0.01	0.02	0.03	0.02	0.02
200	0.05	0.03	0.02	0.04	0.03	0.04
180	0.04	0.01	0.02	0.03	0.02	0.02
140	0.04	0.02	0.02	0.04	0.03	0.03
120	0.04	0.02	0.03	0.03	0.04	0.03
110	0.05	0.02	0.03	0.03	0.04	0.03

2.4 Dimensionless coefficients

The pressure coefficient is defined as [Li, Zhang, Mohammad et al. (2019)]

$$C_p = \frac{p - p_0}{q} = \frac{p - p_0}{0.5 \rho v^2} \tag{4}$$

where p is the static pressure on the model surface, p_0 is the reference static pressure, q is dynamic pressure, ρ is flow density and is dependent of temperature, and v is the flow speed.

The coordinate system defined in EN14067-1 [CEN (2013)] was used in this paper, as shown in Fig. 13. The origin of the coordinate system is defined as: X: middle of the bogies; Y: center of the train between the bogies; Z: at the virtual top of rail.

The moment coefficients C_{Mx}, C_{My}, C_{Mz} are defined as:

$$C_{Mi} = \frac{M_i}{q A_0 d_0}, \ i=x, y, z. \tag{5}$$

The force coefficients C_X, C_Y, C_Z are defined as:

$$C_i = \frac{F_i}{q A_0}, \ i=x, y, z. \tag{6}$$

The rolling moment coefficient around leeward rail C_{MxLee}:

$$C_{MxLee} = C_{Mx} - \frac{C_z b_A}{d_0} \tag{7}$$

where A_0 is reference normalisation area and equals 10 m² for full-scale. d_0 is reference normalisation length and equals 3 m for full-scale. b_A is the lateral contact spacing and equals 1.5 m for full-scale.
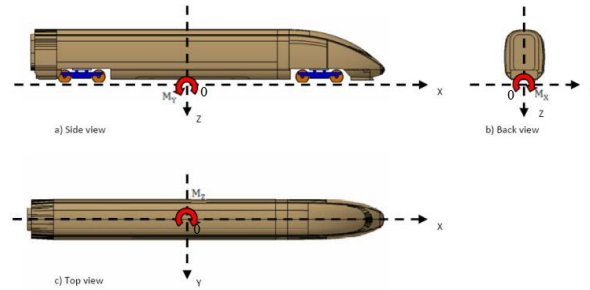
Figure 13: Aerodynamic force and moment reference system

2.5 Arrangement of pressure taps

There are totally 59 pressure taps arranged in Model A (Fig. 14). From that 55 are in the leading car and four in the downstream body. Most of them are in the windward side. Three are in the leeward side for symmetry check.
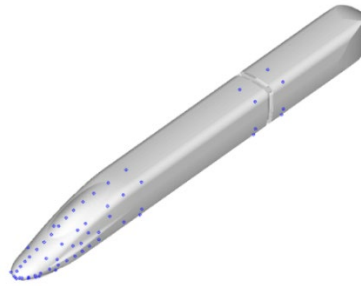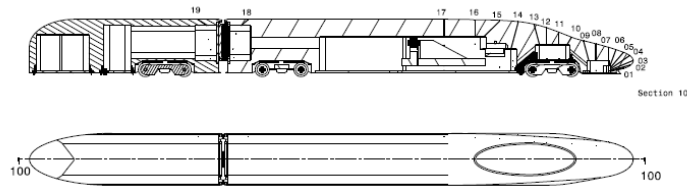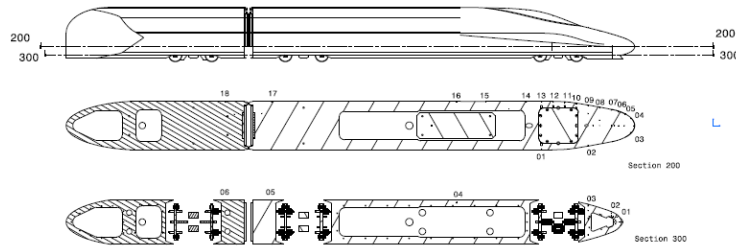

Figure 14: Pressure taps on model A

19 pressure taps are arranged along the centerline are shown in Fig. 15(a). The 3rd is at the foremost location on the nose. It catches the stagnation point at yaw angle of zero.

Two rows of pressure taps are arranged in horizontal planes $0.2703d_0$ and $0.1132d_0$ above the rail, respectively are shown in Fig. 15(b). The rest pressure taps are arranged alone the upper edge and in the side surface are shown in Fig. 16.

(a) Pressure taps on the center line of model A

(b) Pressure taps in two horizontal planes of model A
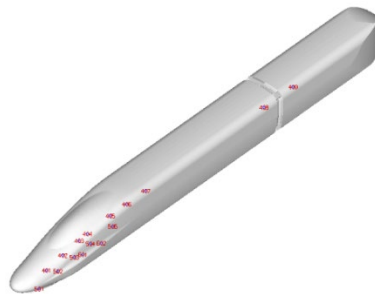
Figure 15: Pressure taps of model A

Figure 16: Pressure taps along the edge and at the side of model A

3 Results and discussion

3.1 Verification of the test set-up

DNW-KKK has been qualified for rolling stock test according to EN147067-6 [CEN (2010)]. The conformity test was performed with a 1:25 scaled ICE3 model at Re of 1 million and temperature of 200 K. Any changes made to the tunnel, including new test set-ups, shall be compared with these data for verification. The measured test results for the reference model C_{mxlee} shall be compared with the conformity data to determine whether the wind tunnel tests are giving results which are within the required tolerances. The target tolerances have been found to be $\varepsilon_{max} = 15\%$ and $\varepsilon_{mean} = 10\%$ for the relevant yaw angles.

Because the model has a scale factor of 1:15, a new test set-up was designed and constructed. A new 1:15 scaled ICE3 model was also manufactured to verify the test set-up.

Before the test with the model began, this 1:15 scaled reference model was tested. The results were shown in Fig. 14. In this diagram the current test result was compared to the data set from EN147067-6 which was acquired with a 1:7 scaled model at Re of 2.3 million and the conformity test data set which was used to qualify the KKK for the cross wind assessment. The three force and moment components as well as the rolling moment around the leeward rail of the three tests match well, especially the side force, rolling and yawing. The difference in drag and lift is relatively large. This is because drag and lift are sensitive to the clearance between the ground and the vehicle underfloor. The ground boundary layer thickness at the model reference point does not correspond to the model

scale, so the effective clearance under the vehicle floor is not the same for the three tests. The deviation to the reference value is defined as:

$$\varepsilon = \left| \frac{C_{mxLee,test} - C_{mxLee,refer}}{C_{mxLee,refer}} \right| \qquad (7)$$
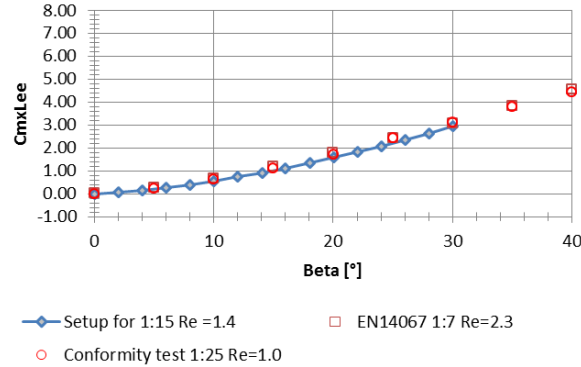

Figure 17: Comparison of the current test results with the EN14067-6 and the conformity test

The result is listed in Tab. 2. The maximal deviation is 8.8%, smaller than the required 15% and the mean deviation is 7.2%, smaller than the required 10%. So the test setup is verified.

Table 2: Deviation of the C_{mxLee} of the current test to the conformity test

Yaw Angle [°]	C_{mxLee} Current Test	C_{mxLee} Conformity	Deviation [%]
10	0.56	0.60	7.70
20	1.57	1.72	8.81
30	2.95	3.11	5.05
max	\	\	8.81
mean	\	\	7.19

3.2 Reynolds number effect on aerodynamic force coefficients

As is well known, an increase in Reynolds number will cause the laminar/turbulent transition point to move upstream and decrease the thickness of the boundary layer. A high Reynolds number may make a separated shear layer reattach to the body, which decreases the width of the wake and weakens the shedding vortex [Schewe and Larsen (1998)]. Therefore, the Reynolds number effect on a car with a streamlined shape should be more significant. Schewe [Schewe (2001)] considered that most global Reynolds number effects on a bluff body are attributable to the structure of the wake, which is changed by the Reynolds number.

The Reynolds number effect of Model A at yaw angle of 0° and 30° are shown in Figs. 18(a)-18(b), respectively.

The drag coefficient of a leading car decreases with higher Reynolds number for yaw angles up to 30°. The drag coefficient drops about 0.06 when the Reynolds number is

raised from 1 million to 10 million. This phenomenon is consistent with the boundary layer theory. The drag consists of skin friction and pressure drag. The pressure drag does not change much with the Reynolds number for small yaw angles. The skin friction decreases with higher Reynolds number.

Since the Reynolds number indicates the extent of the development of turbulence, as the Reynolds number increases, the flow becomes more turbulent. In the process of development from laminar to fully turbulent flow, the velocity gradient close to the wall becomes smaller. As a consequence, the wall shear stress becomes smaller, and the aerodynamic drag of the vehicle thus decreases. When the flow is fully turbulent, the velocity gradient near the wall does not change, and a further increase in Reynolds number does not affect the pressure and velocity distribution at the train's surface, which is represented as the reduced change of the aerodynamic parameters.

The drag coefficient of this high-speed train measured from on-site testing is less than 0.13. It is very close to the drag measured from this wind tunnel test at Reynolds number of 10 million.

The side force coefficient is caused by the high pressure at the windward side and the low pressure generated by the vortex at the lee side. Both pressure distributions are not affected by Reynolds number changes at yaw angles up 30°. This measurement has confirmed this.

The lift coefficient increases with higher Reynolds numbers, though the change is small. At yaw angle of zero the down force is reduced by about 0.03 when the Reynolds number is raised from 1 million to 10 million. At higher yaw angles the lift is reduced about 0.1.

Similar to the side force coefficient, the rolling moment coefficient does not change much with Reynolds numbers.

The magnitude of the pitching moment increases with higher Reynolds number. This indicates that the load on the front bogie is higher at higher Reynolds numbers. The wind tunnel test data is more likely conservative.

The yawing moment coefficient increases with higher Reynolds number. This effect is more evident at higher yaw angles. The yawing moment increases by about 6% when the Reynolds number is raised from 1 million to 10 million.
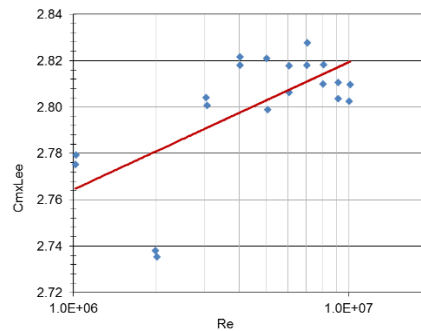
The influence of Reynolds number on the rolling moment coefficient around the leeward rail is relatively smaller. Rolling moment coefficient increases by about 2% when the Reynolds number is raised from 1 million to 10 million.
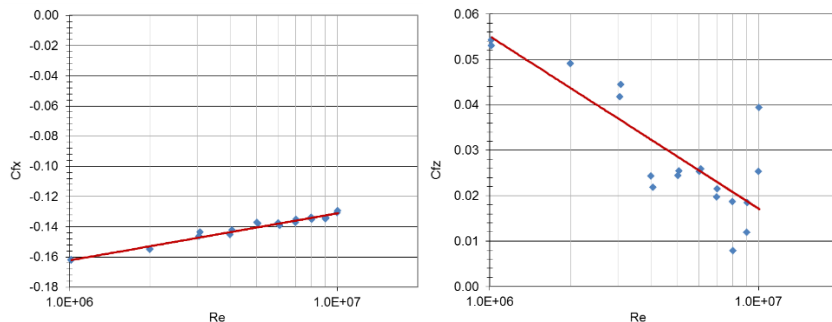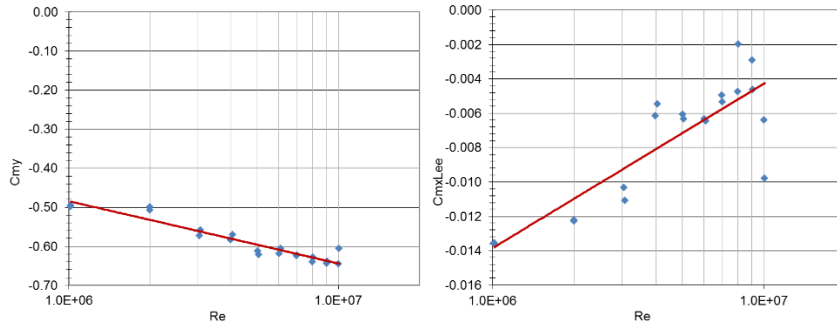
(a) yaw angle=0°
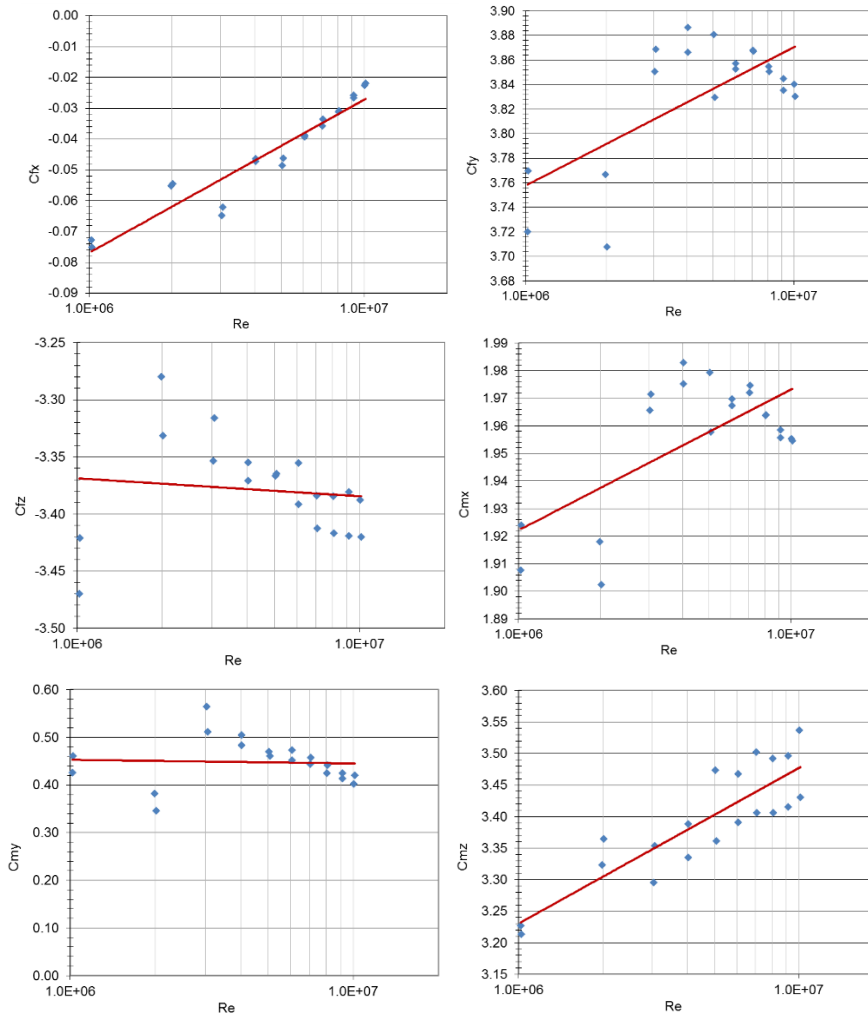
(b) yaw angle=30°

Figure 18: Reynolds number effect of model A at various yaw angle

3.3 Reynolds number effect on the pressure distribution

The three pair symmetrically arranged pressure taps and the pressure taps on the centerline can be used to examine the accuracy of the pressure measurement. For the symmetrically arranged pressure taps the pressure coefficient of the leeward tap at a yaw angle will be compared with its counterpart at an opposite yaw angle. For the pressure taps on the centerline the pressure coefficient at a yaw angle will be compared at an opposite yaw angle. The averaged difference of these check pressure taps of a polar is about 0.005. The standard deviation equals 0.008. The pressure measurement accuracy is therefore high. To obtain an overall pressure distribution on the model, the pressure distributions at the windward side at negative yaw angles were mirrored to the leeward side at the corresponding positive yaw angles.

Fig. 19(a) shows the pressure distribution on the surface of model A at Re of 1 million and yaw angle of 0°. The stagnation point is located at the foremost part of the nose. From this point the flow begins to accelerate. It reaches its maximal velocity at the top of the hood. A separation bubble is formed behind the hood.

Fig. 19(b) shows the pressure distribution at yaw angle of 30°. One can recognize the separation line on the roof of the train.

Fig. 20(a) shows the pressure distribution on the surface of model A at Re of 7 million and yaw angle of 0°. Compared to the pressure distribution at low Reynold number, there is no separation bubble behind the hood. Fig. 20(b) shows the pressure distribution on the surface of model A at Re of 7 million and yaw angle of 30°. At high yaw angles the pressure distribution on the surface of the train is very similar, and the change of Reynolds number is not significant to the pressure distribution on the surface of the train.
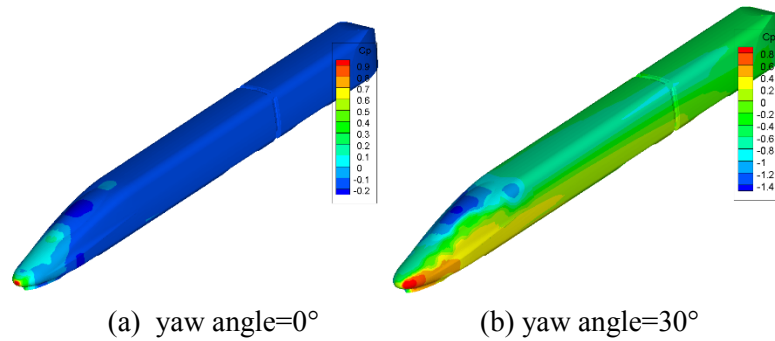
(a) yaw angle=0°   (b) yaw angle=30°

Figure 19: Pressure distribution on surface A at Re=1 million

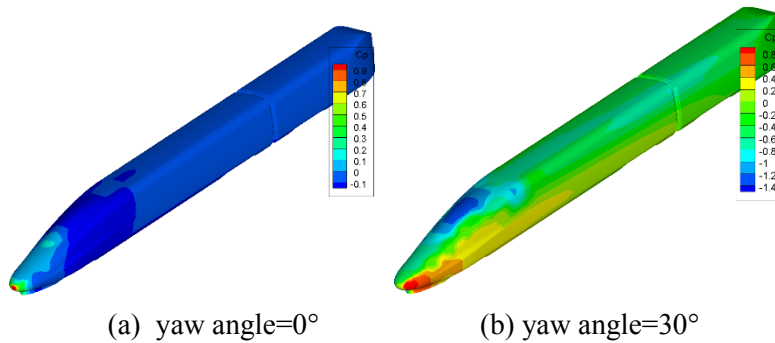(a) yaw angle=0°   (b) yaw angle=30°

Figure 20: Pressure distribution on surface A at Re=7 million

Fig. 21 shows the pressure distributions alone the centerline of Model A at different Reynolds numbers from 2 million to 10 million at yaw angles of 0° and 30°, respectively. Fig. 22 shows the differences of the pressure distributions along the centerline referred to Reynolds number of 2 million. The Reynolds number effect on the pressure distributions alone the centerline is small. Generally speaking, the pressure coefficient increases with higher Reynolds number.

Fig. 23 shows the pressure distributions alone the section 200 at different Reynolds numbers from 2 million to 10 million at yaw angles of 0° and 30°, respectively. Section 200 is at the side of Model A and 0.2703 d_0 above the rail. Fig. 24 shows the differences of the pressure distributions referred to Reynolds number of 2 million. The Reynolds number effect is also not significant on the pressure distributions at the train side. The pressure coefficient increases slightly with higher Reynolds number.
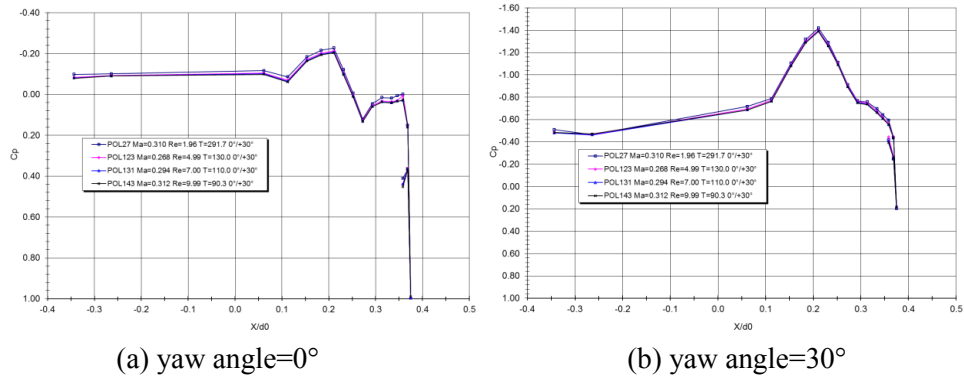
(a) yaw angle=0°   (b) yaw angle=30°

Figure 21: Pressure distributions alone the centerline of Model A

(a) yaw angle=0°   (b) yaw angle=30°

Figure 22: Changes of the pressure alone the centerline of Model A referred to Re=2 million

(a) yaw angle=0°   (b) yaw angle=30°
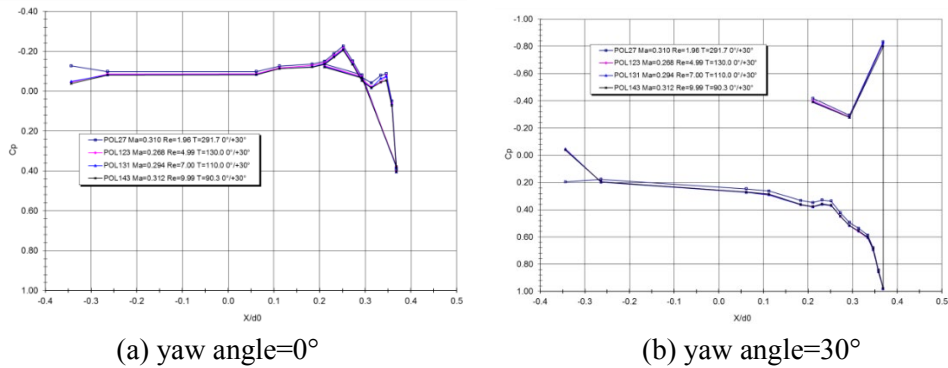
Figure 23: Pressure distributions along the side of Model A (section 200)

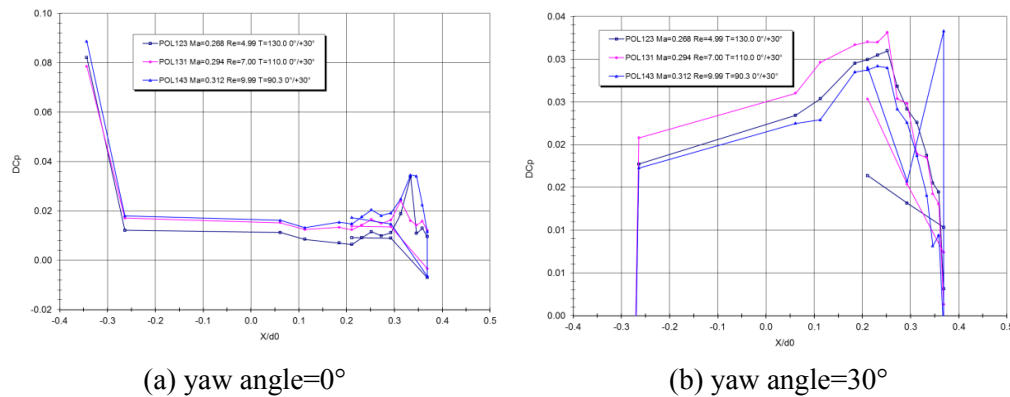|	
(a) yaw angle=0°	(b) yaw angle=30°

Figure 24: Changes of the pressure alone the side of Model A (section 200) referred to Re=2 million

4 Conclusion

A high-speed train model was tested using cryogenic wind tunnel test technology at various Reynolds numbers. By cooling the tunnel down to 90 K the test Reynolds number can be enhanced to 10 million which is the highest Reynolds number a wind tunnel with a train model has ever achieved. It is much closer to the real vehicle Reynolds number of 28 million. The following conclusions were drawn:

For the yaw angle from -30° to +30° the drag decreases with higher Reynolds number. This phenomenon is consistent with the boundary theory. The drag consists of skin friction and pressure drag. The pressure drag does not change much with the Reynolds number for small yaw angles. The skin friction decreases with higher Reynolds number. The drag measured at a Reynolds number of 10 million is very close to the drag measured from on-site testing. The influence of Reynolds number on the other components is not significant.

It is supposed that the influence of the Reynolds number would be significant at higher yaw angles, because the side vortex bursts at higher yaw angle*s*. The yaw angle at which the side vortex breaks up is affected by Reynolds number.

Conflicts of Interest: The authors declare that they have no conflicts of interest to report regarding the present study.

Reference

Ahlefeldt, T.; Koop, L. (2010): Microphone array measurements in a cryogenic wind tunnel. *AIAA Journal*, vol. 48, pp. 1470-1479.

Baker, C. J.; Humphreys, N. D. (1996): Assessment of the adequacy of various wind tunnel techniques to obtain aerodynamic data for ground vehicles in cross winds. *Journal*

of Wind Engineering & Industrial Aerodynamics, vol. 60, pp. 49-68.

Barre, C.; Barnaud, G. (1995): High reynolds number simulation techniques and their application to shaped structures model test. *Journal of Wind Engineering & Industrial Aerodynamics*, vol. 57, pp. 145-157.

Becker, W.; Zhai, J.; Rebstock, R.; Loose, S. (2005): Propeller testing in the cryogenic wind tunnel cologne DNW-KKK. *ICIASF 2005 RecordInternational Congress onInstrum entation in AerospaceSimulation Facilities*, Sendai, Japan, pp. 47-53.

Becker, W.; Rebstock, R.; Loose, S.; Hugues, R.; Raffel, M. (2003): Tests for vehicle aerodynamics in the cryogenic wind tunnel cologne DNW-KKK. *20th International Congress on Instrumentation in Aerospace Simulation Facilities*, pp. 54-58.

Bell, J. R.; Burton, D.; Thompson, M. (2014): Wind tunnel analysis of the slipstream and wake of a high-speed train. *Journal of Wind Engineering & Industrial Aerodynamics*, vol. 134, pp. 122-138.

CEN (2009): *Railway Applications Aerodynamics. Part1: Symbols and units*. BSI.

CEN (2010): *Railway Applications Aerodynamics. Part6: Requirements and Test Procedures for Cross Wind Assessment*, BSI.

Li, T.; Zhang, J. Y.; Mohammad, R.; Yu, M. G. (2019): On the Reynolds-averaged Navier-Stokes modelling of the flow around a simplified train in crosswinds. *Journal of Applied Fluid Mechanics*, vol. 12, no. 2, pp. 551-563.

Li, T.; Hemida, H.; Zhang, J. Y.; Mohammad, R.; Flynn, D. (2018): Comparisons of shear stress transport and detached eddy simulations of the flow around trains. *Journal of Fluids Engineering*, vol. 140, no. 11, pp. 8-12.

Niu, J. Q.; Liang, X. F.; Zhou, D. (2016): Experimental study on the effect of Reynolds number on aerodynamic performance of high-speed train with and without yaw angle. *Journal of Wind Engineering & Industrial Aerodynamics*, vol. 157, pp. 36-46.

Schewe, G. (2001): Reynolds-number effects in flow around more-or-less bluff bodies. *Journal of Wind Engineering & Industrial Aerodynamics*, vol. 89, no. 14, pp. 1267-1289.

Schewe, G.; Larsen, A. (1998): Reynolds number effects in the flow around a bluff bridge deck cross section. *Journal of Wind Engineering & Industrial Aerodynamics*, vol. 74, pp. 829-838.

Schewe, G. (2013): Reynolds-number-effect in flow around a rectangular cylinder with aspect ratio 1:5. *Journal of Fluids and Structures*, vol. 39, pp. 15-26.